Small bottom object density analysis from side scan sonar data by a mathematical morphology detector.

R. Grasso
NATO Undersea Research Centre (NURC)
La Spezia, Italy - grasso@nurc.nato.int

F. Spina
NATO Undersea Research Centre (NURC)
La Spezia, Italy - spina@nurc.nato.int

Abstract - ***This paper describes a system for estimating the local density of small objects on the sea floor by exploiting a robust, non-parametric detector for high resolution images acquired by side scan sonar sensors. Low grazing angle target images are characterised by an area of strong intensity, the highlight, close to an area, the shadow, at the sensor noise level. The detector makes use of mathematical morphology to detect the highlight and the shadow areas within the image, and a fusion scheme to reduce the false alarms due to the sea floor disturbance by declaring a target acquired if an highlight is close to a shadow. Results on data sets collected in the Ligurian and Baltic Sea are reported and discussed.***

Keywords: imaging sonar, signal processing, detection, decision fusion.

1 Introduction

Small bottom object (SBO) local density maps of unknown undersea sites are useful in planning mine hunting missions over these areas in order to maximise the percentage of clearance and at the same time, minimise mission costs. Mission resources can be utilised in an efficient manner, for example, focusing the mission on areas of less SBO density where it is more likely to achieve good mine detection performance with low false alarm rate.

This paper describes a methodology for estimating of the density of SBOs on the seafloor from high resolution data acquired by imaging sonar sensors such as the side scan sonar (SSS). The method relies on an automatic detection system which is based on mathematical morphology (MM) operations [1]. The detector is totally non-parametric and robust against variations of the sea floor and the object intensity signal.

Automatic detection of objects from imaging sonar data is challenging for several reasons. The signal scattered by the sea floor is a non-Gaussian disturbance that is highly non-stationary both in space and time depending on the seafloor roughness and the viewing geometry [2]. Difficulties also arise in modelling the signal received by SBOs due to the wide variety of shapes that may characterise a man-made or natural object. The statistical description of the disturbance and target signals for optimum detection may be unfeasible or may require models that may complicate the architecture of the detector [3].

The non-parametric detector proposed in this paper does not assume any statistical model of the sea floor and the target signals. The constraints on the two signals are quite general and are met in the majority of cases. In particular the object signal at low grazing angles is usually characterised by a highlight area of stronger intensity than the sea floor mean value, close to a shadow area at the sensor noise level. The detector extracts the highlight and the shadow areas from the input image by estimating adaptively the minimum and maximum levels of the seafloor background signal envelope through a series of morphological non-linear filters [1]. The false alarms within the highlight segmentation mask, due to the residuals of the disturbance, are then rejected by fusing the information provided by the shadow mask.

The estimation of the local object clutter density as a function of the position is achieved by simply dividing the surveyed area in squared regions with a pre-defined extent and counting the number of contacts per unit surface in each subset.

The proposed methodology was tested on real data acquired by a ship towed side scan sonar with a central frequency of 455 KHz and by a 900 KHz side scan sonar mounted on board a series of REMUS autonomous underwater vehicles (AUVs). The data sets were gathered on areas located in the Baltic Sea and the Ligurian Sea. The test results indicated positive performance of the detector. A more thorough investigation to asses the detector performance quantitatively is planned.

The section below gives an overview of basic MM; section 3 describes the detector architecture while section 4 reports and discusses the results of side scan sonar data of the Ligurian and the Baltic Sea. Section 5 summarises our conclusions and outlines future developments.

2 Basic mathematical morphology operations

Mathematical morphology (MM) applied to image processing aims at analysing the discrete geometry of objects within the image under study through set theory and topology [1, 4]. It provides a wide range of image to image operations for processing both binary and grayscale images. Such operations works on sets

Report Documentation Page

Form Approved
OMB No. 0704-0188

1. REPORT DATE	2. REPORT TYPE	3. DATES COVERED
JUL 2006		**00-00-2006 to 00-00-2006**

4. TITLE AND SUBTITLE	5a. CONTRACT NUMBER
Small bottom object density analysis from side scan sonar data by a mathematical morphology detector	5b. GRANT NUMBER
	5c. PROGRAM ELEMENT NUMBER
6. AUTHOR(S)	5d. PROJECT NUMBER
	5e. TASK NUMBER
	5f. WORK UNIT NUMBER
7. PERFORMING ORGANIZATION NAME(S) AND ADDRESS(ES) **NATO Undersea Research Centre (NURC),La Spezia, Italy,**	8. PERFORMING ORGANIZATION REPORT NUMBER
9. SPONSORING/MONITORING AGENCY NAME(S) AND ADDRESS(ES)	10. SPONSOR/MONITOR'S ACRONYM(S)
	11. SPONSOR/MONITOR'S REPORT NUMBER(S)

12. DISTRIBUTION/AVAILABILITY STATEMENT
Approved for public release; distribution unlimited

13. SUPPLEMENTARY NOTES
9th International Conference on Information Fusion, 10-13 July 2006, Florence, Italy. Sponsored by the International Society of Information Fusion (ISIF), Aerospace & Electronic Systems Society (AES), IEEE, ONR, ONR Global, Selex - Sistemi Integrati, Finmeccanica, BAE Systems, TNO, AFOSR's European Office of Aerospace Research and Development, and the NATO Undersea Research Centre. U.S. Government or Federal Rights License

14. ABSTRACT
see report

15. SUBJECT TERMS

16. SECURITY CLASSIFICATION OF:			17. LIMITATION OF ABSTRACT	18. NUMBER OF PAGES	19a. NAME OF RESPONSIBLE PERSON
a. REPORT	b. ABSTRACT	c. THIS PAGE			
unclassified	**unclassified**	**unclassified**	**Same as Report (SAR)**	**8**	

defined on a discrete topological space.

For n-dimensional grayscale images with discrete intensities ranging between 0 and M, defined in $\mathbb{N}_0$, the MM transformations operate on the image subgraph. If $\underline{x} \in \mathbb{Z}^n$ is the image pixel position and $f(\underline{x})$ the image intensity value at that position, the subgraph of the image f is defined as follows:

$$SG = \{(\underline{x}, t) \in \mathbb{Z}^n \times \mathbb{N}_0 | 0 \leq t \leq f(\underline{x})\}. \quad (1)$$

In one dimension, SG is the locus of points within the area subtended by the signal graph. The MM operators probe the image subgraph by using a set of known shapes called structural elements (SE) [1]. An n-dimensional image has a subgraph with $n+1$ dimensions (for example, in a two dimensional image there are two spatial dimensions plus one dimension for the image intensity). In general, the SE is an $n+1$ dimensional subset, but a large number of applications make use of flat structuring elements defined in the n-dimensional spatial domain of the image under study. Throughout this work only flat SEs are considered. The shape and the origin of the SE are chosen on the basis of prior knowledge about the relevant or non-relevant structures within the image itself.

The basic MM image to image transformations are erosion and dilation. If $SG(f)$ is the subgraph of a two dimensional image f, for which $t = f(\underline{x})$ is the image discrete intensity at point $\underline{x} \in \mathbb{Z}^2$, and S a flat structuring element, the erosion of $SG(f)$ by S is defined as follows:

$$\epsilon_S[SG(f)] = \left\{(\underline{x}, t) \in \mathbb{Z}^2 \times \mathbb{N}_0 \mid S_{(\underline{x},t)} \subseteq SG(f)\right\}, \quad (2)$$

where $S_{(\underline{x},t)}$ is the structuring element with the origin centred at $(\underline{x}, t)$. The dilation is the dual operation of the erosion and can be defined through the following expression:

$$\delta_S[SG(f)] = \left\{(\underline{x}, t) \in \mathbb{Z}^2 \times \mathbb{N}_0 \mid S_{(\underline{x},t)} \cap SG(f) \neq \phi\right\}. \quad (3)$$

The erode and dilate operations may be implemented as non-linear ordered statistic filters. In particular, the erode is equivalent to a minimum filter while the dilate is equivalent to a maximum filter [1]. A two dimensional image, for example, is processed using a sliding two dimensional window, usually rectangular, which is moved throughout the image domain. The amplitude of the image pixel in the origin of the translated window is substituted with the maximum or the minimum image intensity within the window itself.

Erode and dilate filters can be arranged in order to build new MM operators. Two derived transformations are of particular interest for the present work: the opening and the closing [1]. The opening of an image f, with the structural element S, is defined as the composite of an erosion followed by a dilate with the reflected SE, $\check{S}$, which is the symmetric of S with respect to the origin point:

$$\psi_S[SG(f)] = \delta_{\check{S}}\{\epsilon_S[SG(f)]\}. \quad (4)$$

The closing is the dual transformation, *i.e.* a dilate followed by an erode:

$$\phi_S[SE(f)] = \epsilon_{\check{S}}\{\delta_S[SG(f)]\}. \quad (5)$$

Both opening and closing are used to smooth data. They process the subgraph in two different ways. In particular, opening deletes from the input image subgraph spurious structures having a spatial scale that is smaller than the SE size, while closing fills holes, *i.e.* areas not belonging to the image subgraph, which have a spatial scale that is small compared to the SE size. Opening and closing filters are combined in order to built an MM algorithm which is used to estimate the sea floor signal disturbance from the image data as stated in the following section.

3 The morphological detector

This section describes in details the detector architecture. In particular, section 3.1 gives an overview of the basic sonar signal characteristics that are exploited in order to reduce sea floor disturbance and false alarms after signal segmentation. Section 3.2 introduces the architecture of the MM detector and describes the sea floor background estimation and the fusion scheme used to reduce the false alarm rate.

3.1 Target signal and sea floor disturbance

Small natural or man made objects have various shapes that can be imaged from different grazing and aspect angles. The received object signal may be distorted in several ways depending on the viewing geometry. For these reasons, the detector was designed with the assumption that the exact shape of the object signal is completely unknown except for a set of basic characteristics. An example of SBOs imaged at low grazing angle by a side scan sonar with a central frequency of 455 kHz is depicted in fig. 1. It is clear from this picture and also from fig. 2, showing the range signal of a SBO on a sand seafloor, that the object signal, especially at low grazing angles, has a highlight area of strong intensity, close to a shadow area of low intensity comparable with the sensor noise level. Since the exact shape and size of the objects are unknown, hypotheses on the minimum and maximum size of the objects to be detected will be taken into account. These structural characteristics of the useful signal will be exploited in the detector for reducing the false alarm rate.

For high resolution sensors, the intensity of the sea floor signal can be modelled as a non-Gaussian random process usually characterised by a heavy tailed probability density function (pdf) [2] such as the K or the Generalised-K. The sea floor is highly variable in space, due to the presence of different kinds of sediments, rocky areas, sand ripples, etc., and in time on long scales. This variability implies the non-stationarity of the sea floor signal process and thus the need for a detector that is able to adaptively estimate the disturbance. A parametric detector requires to locally model

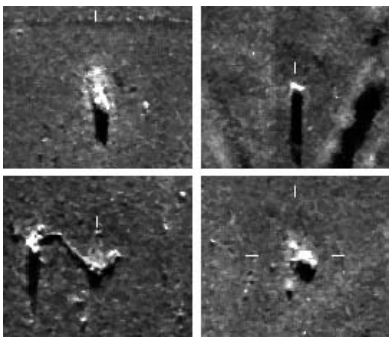

Figure 1: Example of small bottom objects imaged by a side scan sonar.

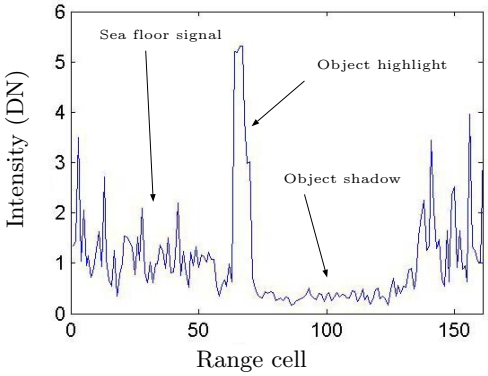

Figure 2: Side scan sonar slant range signal of an object on a sand sea floor.

the pdf of the sea floor process in order to detect a target against the disturbance [5]. On the contrary, non-parametric detectors do not assume any kind of statistical model of the disturbance, resulting in a simpler architecture. In this work, the latter approach was considered. The discrimination between the target and the sea floor is based on the hypothesis that the two signals have a significantly different spatial structure. Statistically, sea floor signal amplitude ranges between a minimum and a maximum envelope level which varies with sea floor characteristics. Locally, in the vicinity of the target signal, the minimum level is usually greater than the target shadow amplitude, while the maximum level is lower than the highlight intensity. Once estimated, the two envelope levels may be used as spatially adaptive thresholds for detecting the highlight and the shadow areas inside an image. The MM processor included in the detector architecture is used, as stated in the following section, for estimating these two levels assuming the target signal as a non-relevant image structure.

3.2 Detector structure

The minimum and maximum envelope levels of the sea floor signal are adaptively estimated, as stylised in fig. 3, by using combinations of two dimensional erode and dilate filters. The detector tracks the disturbance and at the same time, uses the estimated envelope levels as thresholds to segment the input image and produce a mask of highlight and non-highlight areas, and a second mask of shadow and non-shadow areas. The two segmentation masks are then fused together for deleting those highlight areas that are not close to a shadow area, suppressing in this way the residual false alarms due to sea floor disturbance.

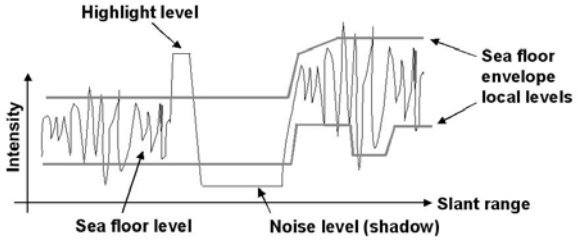

Figure 3: Estimation of sea floor signal maximum and minimum envelopes.

The detector architecture is depicted in fig. 4. The input signal, $s[m,n]$, enters two main branches. The first one estimates the sea floor upper envelope level, $\lambda_h[m,n]$, and detects the highlights. The second branch segments the shadow areas using as threshold the estimation of the minimum sea floor signal level, $\lambda_s[m,n]$. The outputs are binary images where a group of adjacent resolution cells is a binary object. The images from the two branches are fused to suppress those highlight objects which are not close to a shadow object, producing the final detection mask, $m_h[m,n]$, containing highlight objects due to targets with higher confidence than the intermediate highlight mask after the segmentation step.

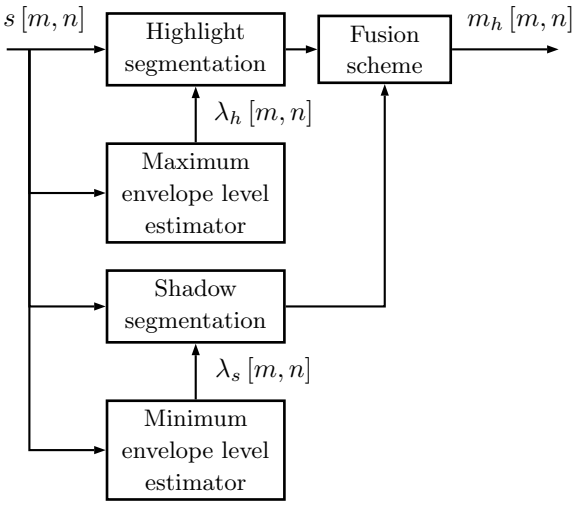

Figure 4: MM detector scheme.

3.2.1 Sea floor envelope level estimator

The sea floor envelopes are estimated by using cascades of opening and closing as depicted in fig. 5 and fig. 6. In particular the sea floor upper level is tracked by filtering the input signal by a closing followed by an opening (fig. 5). The dual filter, that is an opening followed by a closing, is used for the estimation of the minimum envelope level (fig. 6). The SE for both the

estimators is a two dimensional square window with the origin in the centre of the window.

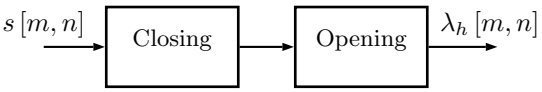

Figure 5: Morphological filters used for estimating the maximum sea floor envelope level.

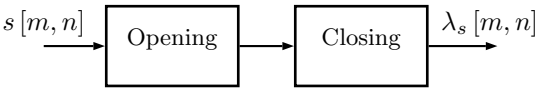

Figure 6: Morphological filters for estimating the minimum sea floor envelope level.

Figures 7 and 8 show the results on a side scan sonar image with a SBO and two types of sea floor, sand and sand ripples. The figure depicts the range signal for a fixed azimuth cell in black and the minimum and maximum envelope levels in red. Figure 7 shows the maximum level estimated by the closing-opening filter with a two dimensional squared filtering window of 23 resolution cells. The output level adaptively follows the sea floor level profile, remaining below the target highlight samples for a large part of the target spatial extent. The estimation of the minimum sea floor envelope by using the opening-closing filter with a square window SE of 15 resolution cells is depicted in fig. 8. The output level tracks the minimum sea floor signal while the samples with an amplitude close to the sensor noise level remain below the output level.

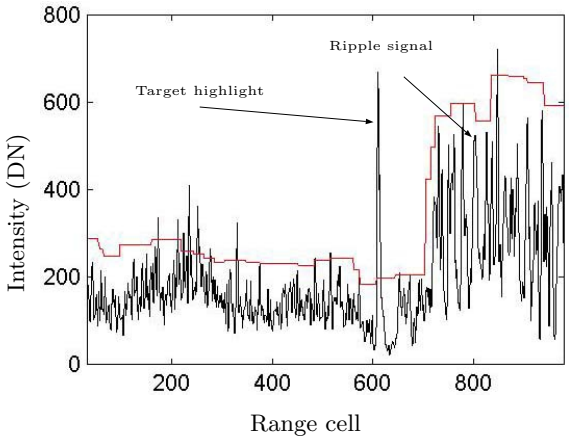

Figure 7: Example of maximum sea floor envelope level estimation (red lines) by morphological processing.

Figure 9 depicts a test image which is used to show how the closing-opening filter processes the input signal in order to estimate the maximum sea floor envelope level. The image (see fig. 9(a)) has been acquired by a SSS with a central frequency of 455 KHz

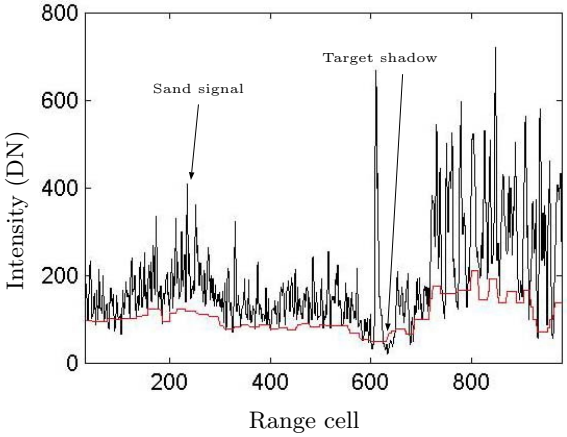

Figure 8: Example of minimum sea floor envelope level estimation (red lines) by morphological processing.

and shows a SBO on a sand sea floor. The resolution is roughly 10 cm for both the slant range and azimuth directions. Figure 9(b) shows the 1D range signal used for demonstrating the filter capabilities. The red line in fig. 9(a) shows the azimuth cell (ping number) along with the signal samples are collected. The target highlight and shadow regions are clearly visible in the graph. The signal is first processed by a dilate

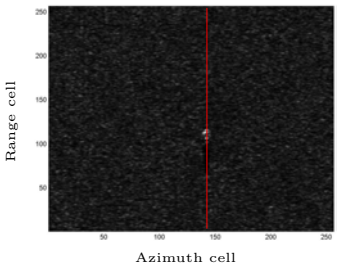

(a)

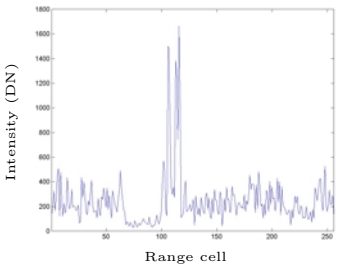

(b)

Figure 9: a) mine like object on sand sea floor; b) range signal relative to the considered azimuth cell.

filter having a linear SE of 23 range cells. Figure 10(a) shows the input signal in blue and the output signal in red. The purpose of the dilate is to filter out the small scale signal structures and to expand the signal subgraph so that the output is always greater than the input signal. The erode transformation (fig. 10(b)) is then used to shrink the signal subgraph in order to make the envelope closer to the original signal enve-

lope.

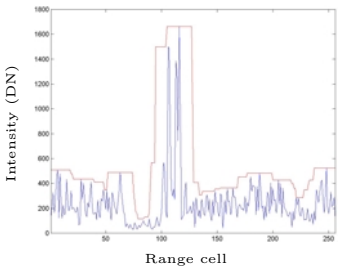

(a)

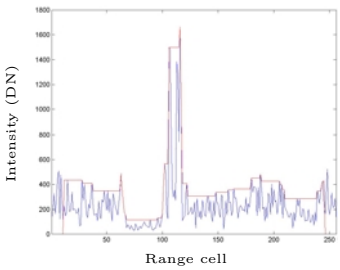

(b)

Figure 10: Closing filtering for the estimation of the maximum sea floor envelope level of the one dimensional signal in fig. 9(b). a) dilate operation. b) erode.

The second step includes an opening operation (fig. 11). The output from the closing filter is first eroded. Figure 11(a) shows the input signal in blue from the closing filter and the result in red. Choosing the filtering window size greater than the maximum highlight object spatial size that can be detected, the output of the erode removes the target structures reducing the highlight amplitude at the local sea floor envelope level. A dilate filter follows in order to expand the subgraph and recover the true signal envelope.

3.2.2 Fusion scheme

As its first processing step, the fusion block enhances the shape of the detected binary highlight and shadow objects by using a series of binary MM operators [1]. The highlight mask is then processed in order to label [1] each binary object so that they can be extracted from the mask. Object shape features, such as the object area or the centre of mass, can now be calculated. The objects with an area which is not in a predetermined range are filtered out. This enhanced highlight mask, namely $m_h^0[m,n]$, is then fused for false alarm reduction with the shadow mask.

The test for the presence of a shadow area close to a binary highlight object is performed by placing a rectangular window near the object position, on the mask $m_h^0[m,n]$, as depicted in fig. 12. The window parameters are the size in along track, W_a, and slant range, W_r, and the length, W_t, of the transition region (see fig. 12). They are set depending on the highlight object size and the maximum elongation of the object shadow area. If the number of shadow resolution cells

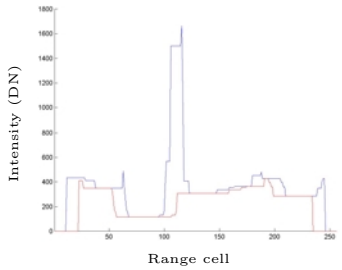

(a)

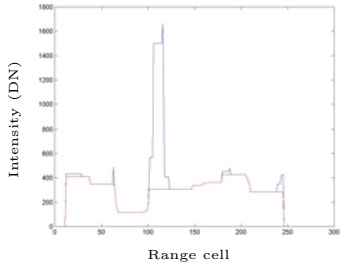

(b)

Figure 11: Opening of the output from the closing filter in fig. 10 with the same SE. a) erode operation b) results of dilate.

in $m_s[m,n]$, within the test window is greater than a fixed percentage of the total number of cells contained in the window itself, then the binary highlight object considered is declared as an acquired target. The test is repeated for each highlight area detected in the mask $m_h^0[m,n]$ in order to produce the final highlight map, $m_h[m,n]$, containing the object declared as targets. The centre of mass of each binary highlight object is then considered for target geo-location and successive SBO density estimation.

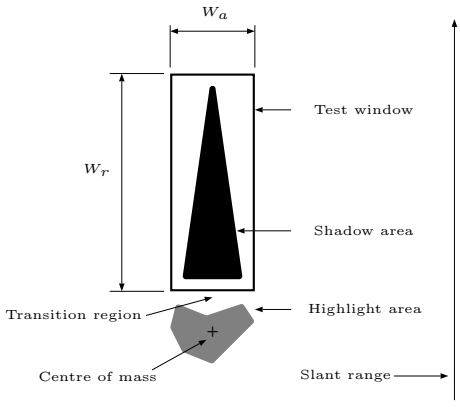

Figure 12: Shadow proximity test window position.

4 Results

This section discusses results from test using data sets acquired in the Ligurian and Baltic Sea by sensors on board REMUS autonomous underwater vehicles

(AUVs) and by ship towed sensors. While the two sites are quite similar with regard to sea floor type, they differ significantly in terms of average SBO density. The SBO local density maps were estimated by dividing each surveyed area into subareas of 25 by 25 meter in order to form a regular grid over the site. The centre mass of the binary objects in $m_h\,[m,n]$ are then geo-referenced and the number of these contacts within each sub-window was divided by the value of the window area in order to estimate the SBO density as a function of the position. The grid of local density is then smoothed by using a two dimensional gaussian filter, with a filtering window of 5×5 grid cells, in order to regularise the density map.

4.1 Detector tests

The MM detector was tested on a set of sample images like the one in fig. 13 showing a SBO on a sand ripple sea floor. The image was acquired in the Ligurian Sea by using a ship towed SSS with a central frequency of 455 kHz. Several test images were extracted from the survey data set in order to asses detector performance qualitatively.

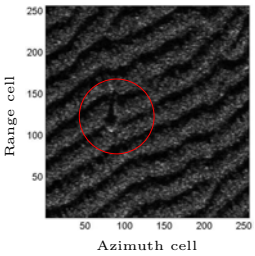

Figure 13: Test image with an SBO on a sand ripple sea floor. Sonar frequency: 455kHz.

Figure 14(a) shows the image highlight detection mask, $m_h^0\,[m,n]$, after highlight labelling and size filtering. The target highlight is clearly visible in the circle. Highlight objects are present, which are false alarms due to sea floor signal samples exceeding the envelope level estimated through the MM processor, are present together with the target. The area covered by the image is approximately 30×30 meter and 70 false alarms were detected after adaptive threshold application.

Figure 14(b) depicts the shadow segmentation mask, $m_s\,[m,n]$. The target shadow (inside the red circle) was correctly retrieved together with the ripple shadow areas.

The two masks are fused in the shadow proximity test block in order to produce the final detection mask, $m_h\,[m,n]$, in which the false alarm objects are completely rejected (see fig. 15). The size of the square filtering windows used in the MM processor was 21×21 and 15×15 resolution cells for the highlight segmentation and the shadow segmentation, respectively. The minimum and the maximum highlight object area were 3×3 and 61×61 resolution cells, respectively. The shadow proximity test parameters used for this test

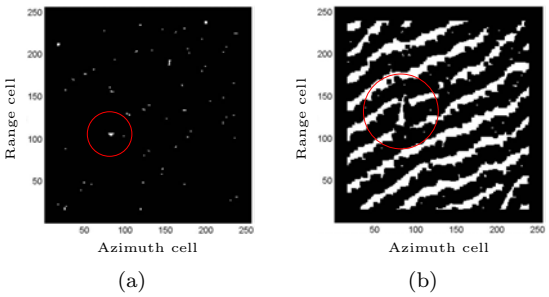

(a) (b)

Figure 14: a) highlight detection mask, $m_h^0\,[m,n]$, after size filtering. b) shadow detection mask $m_s\,[m,n]$.

are $W_a = 50\%$ of the along track highlight object size, $W_r = 31$ range cells and $W_t = 5$ range cells. The test threshold was 50% of the testing window area in number of resolution cells.

The tests revealed that the proposed automatic detection system is robust against sea floor disturbance, reaching good performance in terms of false alarm rates even in the presence of severe environmental conditions such as the location of the target on a sand ripple sea floor. The tests also provided a set of system parameters which were used as reference values for processing other data sets like the ones presented in the following subsections.

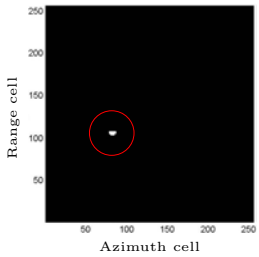

Figure 15: Final detection mask after the shadow proximity test.

4.2 Ligurian Sea data set

The Ligurian Sea data set was acquired on four areas located in a harbour environment, by different REMUS AUVs equipped with a 900 kHz SSS. Dummy targets were deployed on the area of interest and their position were measured and compared with geo-located contacts from the detection system. The analysis of the contacts from the dummy targets yielded an average distance from the nominal target position of 4.5 meter with a standard deviation of 2.2 meter and a minimum and maximum distance value of 2.3 and 9.5 meter respectively.

Figures 16 and 17 show an example of SBO density estimation for one of the acquired SSS data sets. In particular, fig. 16 depicts the AUV mission tracks and the geo-referenced SBO contacts detected by the MM processor. The contacts acquired during this mission were 629 on a surveyed area of $0.077Km^2$. The mean SBO density over the area

is about 3500 $contacts/Km^2$. Figure 17 shows a three dimensional plot of the SBO density as a function of the position. Maximum density on the area is 23000 $contacts/Km^2$ with a standard deviation of 3000 $contacts/Km^2$.

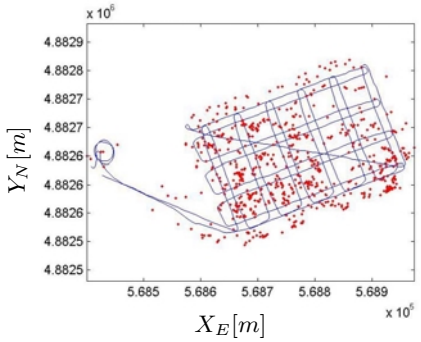

Figure 16: Example of geo-referenced contacts detected by the morphological processor. Projection: UTM. Datum WGS-84.

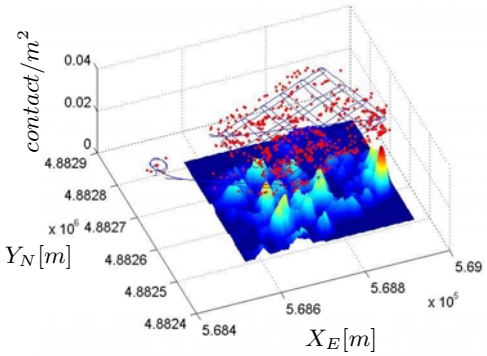

Figure 17: Example of estimated local SBO density map for a data set collected on the Ligurian Sea.

4.3 Baltic Sea data set

The Baltic Sea area is characterised by an higher density of SBOs than the Ligurian Sea area. The survey was composed of a total of 10 AUV missions over different sites. Figure 18 shows the AUV tracks for one of the executed mission and the geo-referenced contacts detected by the MM detector. The mission area is $0.33Km^2$ that is about 4 times the mission area described in the example in section 4.2. A total of 5652 contacts were acquired that is 8 times the number of contacts in the previous example. The average density over the area is 13000 $contacts/Km^2$. A three dimensional view of the local density map is reported in fig. 19. In this case the maximum density is 64000 $contacts/Km^2$ with a standard deviation of 12000 $contacts/Km^2$. Figure 20 shows a two dimensional view of the same map from which it is possible to understand the spatial distribution of the SBOs and the areas of severe density conditions where detecting mines may be challenging.

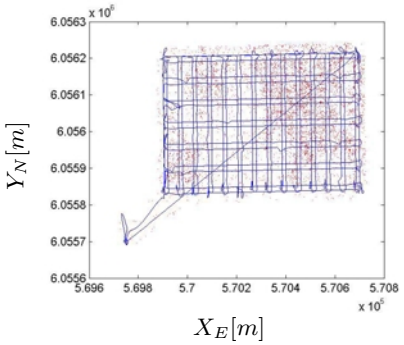

Figure 18: Example of geo-referenced contacts detected for the considered Baltic Sea area. Projection: UTM. Datum WGS-84.

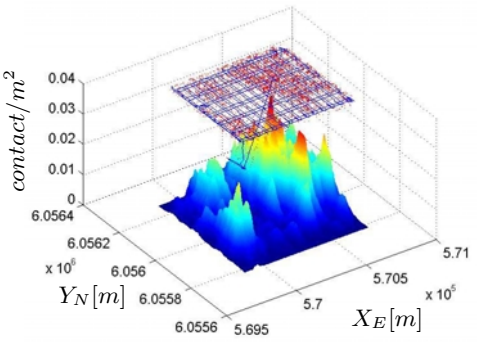

Figure 19: Example of three dimensional local density map for the Baltic Sea area. Projection: UTM. Datum WGS-84.

4.4 Discussion

The results presented here as well as other tests (results not reported in this paper) demonstrated that qualitatively, the proposed MM detector achieves satisfactory rejection of the false alarms due to the sea floor signal even though a priori knowledge about the target signal and the sea floor disturbance is not available. General signal characteristics are only needed, as reported in section 3.1, in order to achieve this performance.

Processing time is another key factor for system performance evaluation. The Baltic Sea data set, for instance, is composed of 652000 sonar pings, about 622

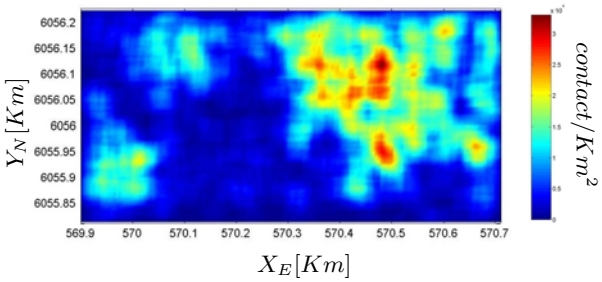

Figure 20: Two dimensional view of the local SBO density map estimated for the Baltic Sea area. Projection: UTM. Datum WGS-84.

MByte, with $8bit/sample$ and 1000 range samples per ping, which is equivalent to 181 hour of mission at $1ping/sec$ sonar rate. Using an optimised system software implementation the entire data set was processed in 2 hours with a throughput of 88 processed ping per second. This throughput allows the system to be used in the framework of rapid environmental assessment (REA), before mine hunting missions, in order to produce a preliminary picture of the surveyed area in near real time.

The local clutter density maps give useful information about the complexity of the surveyed sites and can be used to place mine hunting resources on those areas characterised by low SBO density (see fig 20), where it is more likely to achieve good area clearance.

The clutter density estimation approach used here is extremely simple and is based on the unlikely hypothesis that a target is observed only once during a survey. This is not usually the case, so association of different contacts acquired from the same target should be taken into account. Contact position error assessment is therefore important for correct data association. The analysis of the location error reported in section 4.2 yielded an average error from the measured target position of 4.5 m. In our opinion, this value may be sufficient for correct data association in a moderate SBO density area, as observed in the Ligurian Sea site, by using a simple nearest neighbor algorithm and the estimated contact positions [6]. In denser areas, more sophisticated techniques are probably needed such as the joint probabilistic data association (JPDA) algorithm [6], and possibly in cooperation with other type of sensors.

5 Conclusion and future works

This paper describes a method for estimating the local density of SBO on the sea floor from high resolution sonar images. A MM detector has been designed and implemented to automatically detect SBOs from sonar data. The detector is totally non-parametric and makes use of weak constraints on the useful signal and the disturbance from the sea floor. In particular, cascades of MM non-linear filters are used for estimating the minimum and the maximum envelopes of the sea floor signal in order to segment the input image in its highlight and shadow components. The segmentation is followed by a shadow proximity test for reducing false alarms in the highlight mask due to residual sea floor disturbances. The acquired target contacts are then geo-referenced and used for estimating the local object clutter density over the area of interest. The MM detector system is characterised by a good false alarm rejection rate as qualitative tests performed on sand and sand ripple sea floor images showed. The low processing burden of the detector system makes the proposed methodology suitable for deployment on REA missions for which rapid delivery of results is a fundamental requirement.

Future investigations should be focused on two main tasks. The first is the assessment of detector performance through an experimental evaluation of the receiver operating characteristic (ROC) curves. The analysis has to take into account different scenarios in order to provide a set of ROC curves as a function of sea floor type and of detector parameters such as the size of the MM filtering windows and the shadow proximity test threshold. This investigation is fundamental in enabling the selection of detector parameters that will produce a desired false alarm and detection rate. In addition, this analysis may suggest useful ways for improving overall system performance and to obtain a more robust and reliable SBO local density estimation.

The second task concerns the problem of data association. A target may be observed more than once during a survey so the detected contacts from the same target have to be associated in order to not bias the estimation of the SBO local density. For this reason, the integration of the MM detector into a concurrent mapping and localization (CML) algorithm [7] which will take care of data association, object initiation, maintenance and deletion, and vehicle state prediction and estimation is currently under study.

References

[1] Pierre Soille. *Morphological Image Analysis: Principles and Applications*. Springer-Verlag New York, Inc., Secaucus, NJ, USA, 2003.

[2] Griffiths H., Dunlop J., and Voles R. Texture analysis of side scan sonar imagery using statistical scattering models. In *High Frequency Acoustics in Shallow Water*, Lerici, Italy, June 1997. NATO Undersea Research Centre.

[3] Reed Scott, Petillot Yvan, and Bell Judith. An automatic approach to the detection and extraction of mine features in side scan sonar. *IEEE Journal of Oceanic Engineering*, 28(1):90–105, January 2003.

[4] Batman S. and Goutsias J. Unsupervised iterative detection of land mines in highly cluttered environments. *Image Processing, IEEE Transactions on*, 12(5):509 – 523, May 2003.

[5] Steven M. Kay. *Fundamentals of statistical signal processing*. Prentice Hall signal processing series. 1993.

[6] S. Blackman and R. Popoli. *Design and Analysis of Modern Tracking Systems*. Artech House, 1999.

[7] Gamini Dissanayake M. W. M., Newman P., Clark S., Durrant-Whyte H. F., and Csorba M. A solution to the simultaneous localization and map building (SLAM) problem. *Robotics and Automation, IEEE Transactions on*, 17(3):229 – 241, June 2001.